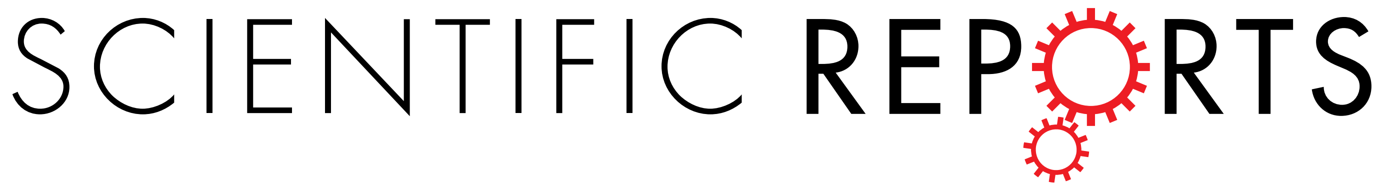

OPEN

Maskless inverted pyramid texturization of silicon

Yan Wang[1,*], Lixia Yang[1,*], Yaoping Liu[1,*], Zengxia Mei[1], Wei Chen[1], Junqiang Li[1], Huili Liang[1], Andrej Kuznetsov[2] & Du Xiaolong[1]

Received: 18 February 2015
Accepted: 01 May 2015
Published: 02 June 2015

We discovered a technical solution of such outstanding importance that it can trigger new approaches in silicon wet etching processing and, in particular, photovoltaic cell manufacturing. The so called inverted pyramid arrays, outperforming conventional pyramid textures and black silicon because of their superior light-trapping and structure characteristics, can currently only be achieved using more complex techniques involving lithography, laser processing, etc. Importantly, our data demonstrate a feasibility of inverted pyramidal texturization of silicon by maskless Cu-nanoparticles assisted etching in $Cu(NO_3)_2$ / HF / H_2O_2 / H_2O solutions and as such may have significant impacts on communities of fellow researchers and industrialists.

Silicon texturization is an important topic of modern science and technology, particularly appealing in photovoltaics (PV)[1–3]. Random pyramid arrays with a reduced reflectivity of 10% can be readily obtained via anisotropic etching of (100)-oriented crystalline silicon (c-Si) in alkaline solutions[4], which is widely used in c-Si PV cell manufacturing[5–7].The black silicon (B-Si) with even lower reflectivity, down to 2%, is widely obtained by metal-assisted chemical etching[8]. However, B-Si is still not suitable for PV cells because of its high recombination rates due to the nanostructures[9]. The so-called inverted pyramid arrays, outperforming pyramid arrays and B-Si in PV because of their superior light-trapping and structure characteristics[10–12], can currently only be achieved using more complex techniques involving lithography, laser processes, etc[13–18]. This complexity and corresponding extra costs hinder the implementation of inverted pyramidal structures in mass production. Here, we demonstrate the use of maskless Cu-nanoparticles (NPs) assisted anisotropic etching of c-Si in $Cu(NO_3)_2/HF/H_2O_2/H_2O$, resulting in excellently performing inverted pyramidal arrays. Importantly, we do not only report a unique technical solution but uncover the underlying mechanisms, interdisciplinary in nature. In particular, due to a limited electron capturing ability of Cu^{2+} and a difference of electron supplying rates in Si (100) and (111) planes, Cu-NPs population as attached to c-Si, appear to be a function of the crystallographic plane orientation. Tuning the density of Cu-NPs on Si (100) and (111) planes naturally allows sui generis carrier transport balance enabling the anisotropic etching. Notably, our technique is compatible with a majority of PV production lines and as such may trigger a new era of using inverted pyramidal texturization of Si.

Results and Discussion

Wafer-scale arrays of Si inverted pyramids were fabricated via a Cu-NPs-assisted anisotropic etching technique in a $Cu(NO_3)_2/HF/H_2O_2/H_2O$ mixture at 50 °C. The underlying principles are based on the electrochemical reaction between Si and Cu^{2+}/Cu-NPs[19,20]. The driving force of this electrochemical reaction is the electrochemical potential difference between Si and Cu^{2+}/Cu-NPs. The reaction can be described as two half-cell reactions just like the well-known metal-assisted chemical etching method for fabricating various Si nanostructures[21–25].

[1]Key Laboratory for Renewable Energy, Beijing Key Laboratory for New Energy Materials and Devices, National Laboratory for Condensed Matter Physics, Institute of Physics, Chinese Academy of Sciences, Beijing, 100190, China. [2]Department of Physics, Centre for Materials Science and Nanotechnology, University of Oslo, PO Box 1048 Blindern, Oslo, NO-0316, Norway. *These authors contributed equally to this work. Correspondence and requests for materials should be addressed to Y.L. (email: ypliu@iphy.ac.cn) or X.D. (email: xldu@iphy.ac.cn)

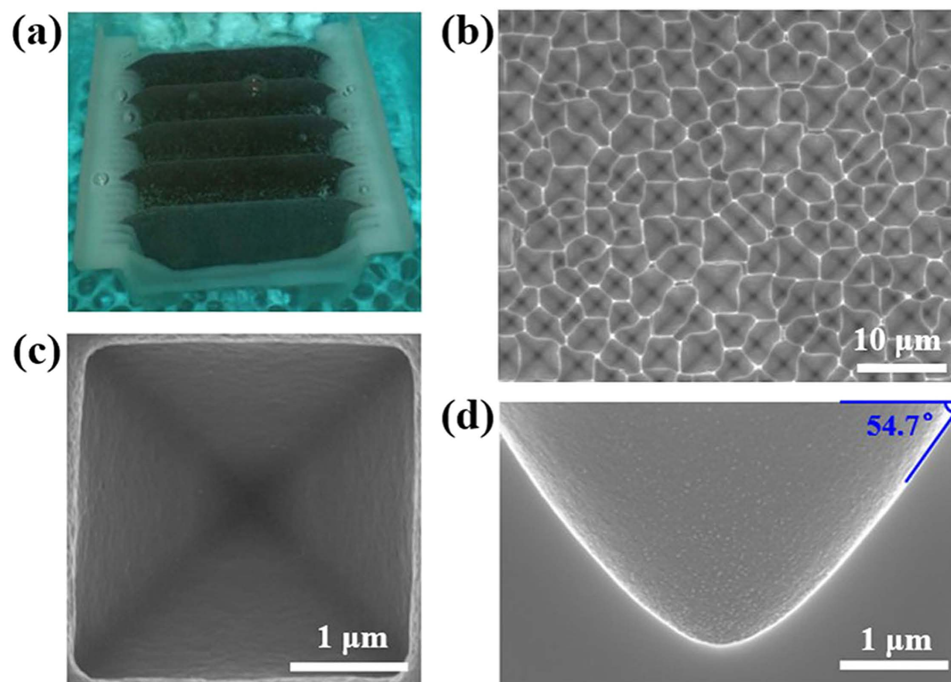

Figure 1. A photo of Cu-NPs-assisted etching process and SEM images. (**a**) 156 mm × 156 mm c-Si wafers being etched in a $Cu(NO_3)_2/HF/H_2O_2/H_2O$ etching bath. (**b**) SEM top-view image of the inverted pyramid arrays for 15 min processing. (**c**) Magnified SEM top-view image of an individual inverted pyramid processed for 15 min. (**d**) SEM cross-sectional view of an individual inverted pyramid processed for 15 min.

Cathode reaction:

$$Cu^{2+} + 2e^{-}_{VB} \rightarrow Cu^{0}(s) \quad (1)$$

$$H_2O_2 + 2H^{+} \rightarrow 2H_2O + 2h^{+} \quad (2)$$

Anode reaction:

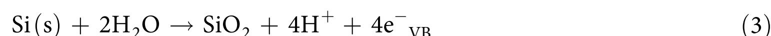

$$Si(s) + 2H_2O \rightarrow SiO_2 + 4H^{+} + 4e^{-}_{VB} \quad (3)$$

$$SiO_2(s) + 6HF \rightarrow H_2SiF_6 + 2H_2O \quad (4)$$

In this case, the $Si/Cu(NO_3)_2/H_2O_2/HF$ system is composed of a corrosion-type redox couple: the cathodic reduction of Cu^{2+} ions with H_2O_2 as well as the anodic oxidation and dissolution of Si beneath the deposited Cu-NPs. Cu^{2+} ions capture electrons from the vicinity of the Si substrate, aggregate and form NPs. In this manner, Cu-NPs nucleated originally on the Si surface attract electrons from Si and become negatively charged because Cu is more electronegative than Si. These negatively charged Cu-NPs grow further by attracting the Cu^{2+} ions from the solution[19,20,26]. During this process, Si atoms underneath the Cu-NPs are continuously oxidized and etched by the HF. Simultaneously, the reduction of H_2O_2 on the Cu-NPs is indispensable to induce anisotropic Cu-NPs' deposition onto the Si surface and guarantee the formation of inverted pyramid arrays, which will be interpreted in the following sections. The inverted pyramid arrays were cleaned using concentrated nitric acid in a sonication bath for at least 20 min to remove all of the residual Cu-NPs. After the nitric acid bath, no Cu-NPs were observed by scanning electron microscopy (SEM) analysis and no Cu peaks appeared in the energy-dispersive X-ray spectra of the inverted pyramid arrays.

The inverted pyramid arrays fabricated using this approach were regular and consistent throughout the batches and across large areas, up to wafer-scale. Fig. 1(a) shows a photo of several 156 mm × 156 mm Si (100) wafers being etched in the $Cu(NO_3)_2/HF/H_2O_2/H_2O$ solution. The cross-sectional SEM image of the inverted pyramid shown in Fig. 1(d) reveals that the angle between the facet of the inverted pyramid and the (100) surface is 54.7°, indicating that the facets are terminated with Si (111) planes. As shown in Fig. 1(b), the inverted pyramid arrays are random because of the original irregular morphology and saw damage on Si; however, the surface is fully covered by random inverted pyramids and is regular when considered as a whole. The length of the inverted pyramids' bottom side varies within 2–6 μm, and the

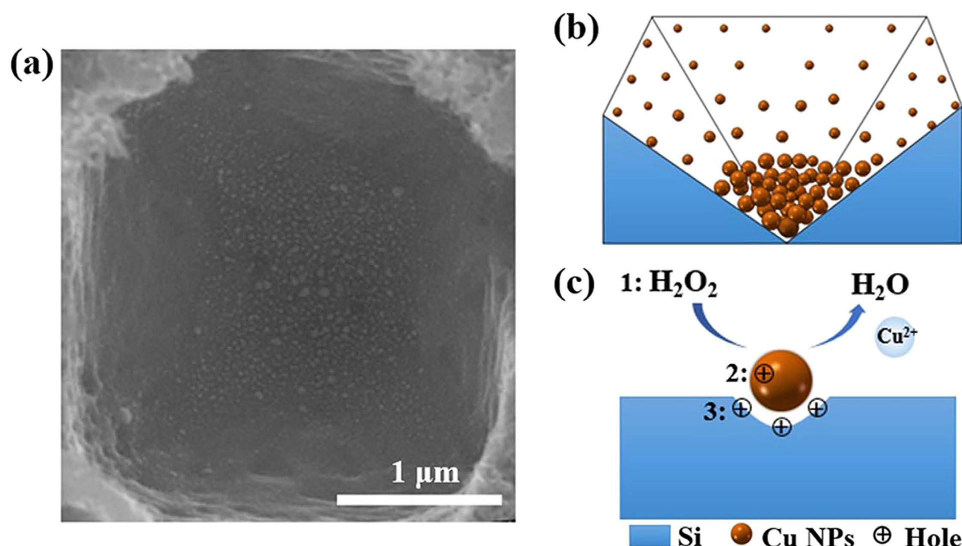

Figure 2. SEM image and schematics of Cu NPs assisted anisotropic etching. (**a**) SEM top-view image of an individual inverted pyramid via etching for 1 min. (**b**) Schematics of the anisotropic deposition of Cu NPs. (**c**) Schematics of the H_2O_2 reduction process and the mechanisms for the holes injection.

etching depth is in the range of 1–5 µm. Fig. 1(c) shows a standard inverted pyramid with (111) sidewalls. The key parameters of the reaction were identified using p-type (100)-oriented, nominally 1-3 Ω cm c-Si as the etching wafer, but the process was successfully tested for n-type material too, naturally adjusting the solvent. In general, the morphology of the inverted pyramid arrays was well controlled by adjusting the etching time, the concentration of $Cu(NO_3)_2/HF/H_2O_2$ and the etching temperature.

Up to date, the anisotropic wet chemical etching of c-Si has been done in alkaline solutions, resulting in random pyramid arrays, whereas isotropic wet chemical etching is commonly observed in HF based solutions[4]. In our technique, the anisotropic deposition of Cu-NPs from the $Cu(NO_3)_2/HF/H_2O_2/H_2O$ mixture is the key step in the synthesis of the inverted pyramid arrays without any mask. In Fig. 2(a), the early form of one inverted pyramid is demonstrated, where more and larger Cu-NPs are observed on Si (100) surface and fewer and smaller Cu-NPs are observed on Si (111) surfaces. This orientation-dependent population of Cu-NPs occurs due to a low reduction potential of Cu^{2+}, exhibiting a limited ability to withdraw electrons directly from Si at room temperature[27]. Notably, rising temperature (to 50 °C) enhances the probability of the electron capturing by Cu^{2+} ions, leading to the nucleation of Cu-NPs on c-Si. Importantly, the electronic properties of (100) and (111) planes in c-Si are different in terms of the surface bond densities[4,28,29]. Accounting that, the number of electrons "available" on Si (100) planes is greater than that on the Si (111) planes, Cu-NPs preferentially nucleate on Si (100) plane because of the higher probability of electron capturing by Cu^{2+} ions. Further growth may be facilitated by the interaction between Cu^{2+} ions and these negatively charged Cu-NPs, resulting in faster growth of Cu-NPs on Si (100) plane than that on (111) planes. Fig. 2(b) is a simulated diagram that shows the pattern of anisotropic Cu-NPs' deposition. As a result, Si atoms underneath the Cu-NPs are preferentially oxidized and then etched by HF, leading to a faster etching along Si $<100>$ directions.

Notably, H_2O_2 plays an important and special role in the selective etching too, as previously mentioned. Energetically, the electrochemical potential of H_2O_2 is much more positive than either the valence band of Si or the reduction potential of Cu^{2+}/Cu-NPs. Thus, the presence of H_2O_2 may promote holes injection into the valence band of Si as well as into the Cu-NPs. Although the Si etching by HF does occur when a Si substrate is subjected to an HF/H_2O_2 solution, the etching rate is less than 10 nm/h in an etchant with a high concentration of H_2O_2. In practice, the presence of a noble metal is necessary for accelerating Si etching in HF/H_2O_2 solutions[22]. In other words, the observed preferential reduction of H_2O_2 is attributed to the surface of the metal rather than to the surface of the bare Si[22]. Therefore, the reduction of H_2O_2 (labeled as "1" in Fig. 2(c)) in the $Si/Cu(NO_3)_2/H_2O_2/HF$ system is likely to occur on the surface of the Cu-NPs too. When moderate amounts of H_2O_2 are introduced, Cu-NPs are deposited anisotropically, which assists in the etching of inverted pyramids by HF; thus, the injected holes are consumed via two pathways. The holes are consumed by the Cu-NPs, ensuring kinetic equilibrium between the deposition and dissolution of Cu NPs (as labeled by "2" in Fig. 2c). Some holes also diffuse through the Cu-NPs and are injected into the Si substrate (labeled by "3" in Fig. 2c) selectively accelerating the etching of c-Si beneath the Cu-NPs.

In the absence of H_2O_2, the reduction of Cu^{2+} will be faster, allowing more Cu-NPs to be formed at the Si surface because of unlimited supply of Cu^{2+} ions. The Cu-NPs quickly grow larger and cover the majority of the Si wafer surface[30]. This situation induces overlapping regions of oxidation and,

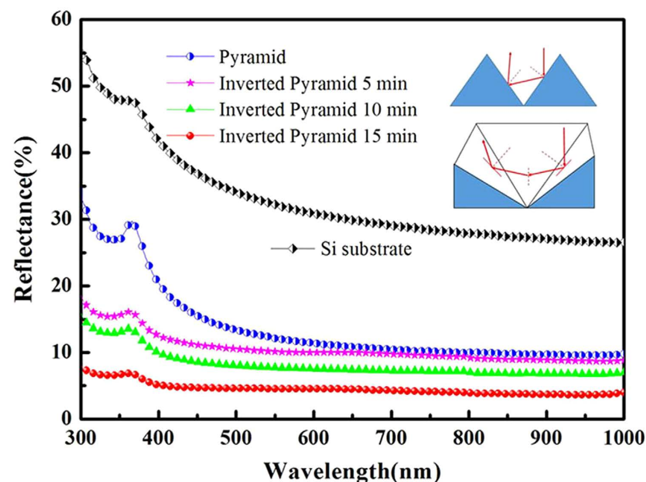

Figure 3. Reflectance spectra of pyramid arrays and the inverted pyramid arrays obtained via Cu NPs assisted anisotropic etching for 5 min, 10 min and 15 min. The inset shows schematics of the light path in the normal pyramidal structure and an individual inverted pyramid before being reflected away.

accordingly, faster isotropic Si etching. A thin Cu film will be formed very quickly at 50 °C; this film will inhibit the etching of Si by acting as a barrier between the Si and the etchants. At high concentrations of H_2O_2, the oxidation of Cu-NPs is faster than the reduction of Cu^{2+}, resulting in the deposition of a few small Cu-NPs randomly on the Si surface; therefore, the original morphology of the Si does not substantially change, except for the formation of a few shallow nano-pits. On the basis of the interaction between H_2O_2 and Cu-NPs and their roles in the process, inverted pyramid arrays were obtained for the first time using a simple and low-cost maskless chemical etching.

After the etching process, the hemispheric total reflectance for normal incidence was measured using a Varian Cary 5000 spectrophotometer with an integrating sphere. The reflectance spectra of the inverted pyramid arrays prepared using different etching times are shown in Fig. 3, illustrating the tunability of our technique. Notably, our texturization reduced the mean reflectivity of c-Si (over the wavelength range from 300 to 1000 nm) down to ~4.4% without any antireflective coating as compared to much higher reflectivity from the normal pyramid arrays (see Fig. 3). The short wavelength spectral response analysis indicates that approximately 37% of the incoming light undergoes a triple bounce due to its interaction with the adjoining planes of the inverted pyramid geometry before being reflected away[11]. As shown in the inset in Fig. 3, the incident light, which strikes one face of the inverted pyramid, is reflected (the first bounce) onto an orthogonal plane, which is then reflected (the second bounce) onto the face complementary to the original point of impact and finally reflected away (the third bounce), while a double bounce of most incident light was observed in the pyramid geomtry[11]. The triple bounce increases the path length of the light, which induces an increased absorption of the incident light. The reduced front surface reflectance, together with the increased light absorption, makes inverted pyramid arrays an attractive and efficient light-trapping geometry. Moreover, the recessed structure is more suitable for covering and filling, such as for the coverage of amorphous Si in heterojunction solar cells and the filling of metal electrodes in photovoltaic devices.

In summary, we discovered a method of maskless texturization of c-Si with so-called inverted pyramid arrays that can be immediately uptaken for industrialization. In comparison with the pyramidal structure, which is widely used for Si solar cells, the inverted pyramidal structure has the same micrometer scale but lower reflectivity and higher light absorption, along with a shorter etching time and a lower etching temperature during the texturing process; compared with the B-Si obtained by the noble metal assisted chemical etching, inverted pyramidal structures are achieved by the cheaper metal, Cu-NPs assisted chemical etching. Moreover, inverted pyramid not only has superior structural characteristic but also ensures low recombination rates. Furthermore, the generality and scalability of our technique are very promising for the fabrication of other advanced Si-based devices. Last but not least, the underlying principles governing the etching process are understood. In particular, the preferential etching along <100> directions is realized by a charge transfer assisted with Cu-NPs.

Methods

Inverted pyramid arrays were originally etched from commercial 156 mm × 156 mm, boron-doped (1-3 Ω cm), (100)-oriented c-Si wafers via Cu NPs assisted anisotropic etching. Before being etched in the solution, the wafers were thoroughly rinsed in acetone to remove any organic contaminants and then rinsed with deionized water. The inverted pyramid arrays were obtained when the wafers were etched for 15 min at 50 °C in a polytetrafluoroethylene container filled with 5 mM $Cu(NO_3)_2$, 4.6 M HF and 0.55 M

H_2O_2. Residual Cu-NPs were removed using concentrated nitric acid in a sonication bath for at least 20 min. The Si wafers were thoroughly rinsed with deionized water and dried under flowing nitrogen. The morphologies and structures of the wafers were characterized using a Hitachi S-4800 scanning electron microscope. The hemispheric total reflectance for normal incidence was measured using a Varian Cary 5000 spectrophotometer with an integrating sphere.

References

1. Moreno, M., Daineka, D. & Cabarrocas, P. R. Plasma texturing for silicon solar cells: From pyramids to inverted pyramids-like structures. *Sol. Energy Mater. & Sol. Cells* **94,** 733–737 (2010).
2. Huynh, W. U., Dittmer, J. J. & Alivisatos, A. P. Hybrid nanorod-polymer solar cells. *Science* **295,** 2425–2427 (2002).
3. Law, M., Greene, L. E., Johnson, J. C., Saykally, R. & Yang, P. Nanowire dye-sensitized solar cells. *Nature Mater*. **4,** 455–459 (2005).
4. Seidel, H., Csepregi, L., Heuberger, A. & Baumgärtel, H. Anisotropic Etching of Crystalline Silicon in Alkaline Solutions. *J. Electrochem. Soc.* **137,** 3612–3626 (1990).
5. Singh, P. K., Kumar, R., Lal, M., Singh, S. N. & Das, B. K. Effectiveness of anisotropic etching of silicon in aqueous alkaline solutions. *Sol. Energy Mater. & Sol. Cells* **70,** 103–113 (2001).
6. Campbell, P. & Green, M. A. Light trapping properties of pyramidally textured surfaces. *J. App. Phys*. **62,** 243–249 (1987).
7. Vazsonyi, E. *et al.* Improved anisotropic etching process for industrial texturing of silicon solar cells. *Sol. Energy Mater. & Sol. Cells* **57,** 179–188 (1999).
8. Liu, X. G. *et al.* Black silicon: fabrication methods, properties and solar energy applications. *Energy Environ. Sci.* **7,** 3223–3263 (2014).
9. Oh, J., Yuan, H. C. & Branz, H. M. An 18.2%-efficient black-silicon solar cell achieved through control of carrier recombination in nanostructures. *Nature Nanotechnol*. **7,** 743–748 (2012).
10. Mavrokefalos, A., Han, S. E., Yerci, S., Branham M. S. & Chen, G. Efficient Light Trapping in Inverted Nanopyramid Thin Crystalline Silicon Membranes for Solar Cell Applications. *Nano Lett*. **12,** 2792–2796 (2012).
11. Smith, A. W. & Rohatgi, A. Ray tracing analysis of the inverted pyramid texturing geometry for high efficiency silicon solar cells. *Sol. Energy Mater. & Sol. Cells* **29,** 37–49 (1993).
12. Zhao, J. H., Wang, A. H. & Green, M. A. 24.5% Efficiency Silicon PERT Cells on MCZ Substrates and 24.7% Efficiency PERL Cells on FZ Substrates. *Prog. Photovolt: Res. Appl*. **7,** 471–474 (1999).
13. You, J. S. *et al.* Experiments on anisotropic etching of Si in TMAH. *Sol. Energy Mater. & Sol. Cells* **66,** 37–44 (2001).
14. Fan, Y. J. *et al.* Differences in etching characteristics of TMAH and KOH on preparing inverted pyramids for silicon solar cells. *Appl. Surf. Sci.* **264,** 761–766 (2013).
15. Sun, C. H., Min, W. L., Linn, N. C. & Jiang, P. Templated fabrication of large area subwavelength antireflection gratings on silicon. *Appl. Phys. Lett*. **91,** 231105 (2007).
16. Kumar, K., Lee, K. K. C., Herman, P. R., Nogami, J. & Kherani, N. P. Femtosecond laser direct hard mask writing for selective facile micron-scale inverted-pyramid patterning of silicon. *Appl. Phys. Lett*. **101,** 222106 (2012).
17. Lin, J. W., Liu, E. T., Wu, C. H., Hsieh, I. J. & Chao, T. S. Formation of inverted-pyramid structure by modifying laser processing parameters and acid etching time. *ECS Trans*. **35,** 67–72 (2011).
18. Chaturvedi, N., Hsiao, E., Velegol, D. & Kim, S. H. Maskless Fabrication of Nanowells Using Chemically Reactive Colloids. *Nano Lett*. **11,** 672–676 (2011).
19. Huang, Z. P., Geyer, N., Liu, L. F., Li, M. Y. & Zhong, P. Metal-assisted electrochemical etching of silicon. *Nanotechnology* **21,** 465301 (2010).
20. Zheng, H. *et al.* Porous silicon templates prepared by Cu-assisted chemical etching. *Mater. Lett.* **118,** 146–149 (2014).
21. Peng, K. Q. *et al.* Metal-Particle-Induced, Highly Localized Site-Specific Etching of Si and Formation of Single-Crystalline Si Nanowires in Aqueous Fluoride Solution. *Chem. Eur. J*. **12,** 7942–7947 (2006).
22. Huang, Z. P., Geyer, N., Werner, P., Boor, J. D. & Gösele, U. Metal-Assisted Chemical Etching of Silicon: A Review. *Adv. Mater.* **23,** 285–308 (2011).
23. Peng, K. Q. *et al.* Fabrication of Single-Crystalline Silicon Nanowires by Scratching a Silicon Surface with Catalytic Metal Particles. *Adv. Funct. Mater.* **16,** 387–394 (2006).
24. Tian, B. Z. *et al.* Coaxial silicon nanowires as solar cells and nanoelectronic power sources. *Nature* **449,** 885–888 (2007).
25. Liu, Y. P. *et al.* Nanostructure Formation and Passivation of Large-Area Black Silicon for Solar Cell Applications. *Small* **8,** 1392–1397 (2012).
26. Morinaga, H., Suyama, M. & Ohmi, T. Mechanism of Metallic Particle Growth and Metal-Induced Pitting on Si Wafer Surface in Wet Chemical Processing. *J. Electrochem. Soc.* **141,** 2834–2841 (1994).
27. Lu, Y. T. & Barron, A. R. Anti-reflection layers fabricated by a one-step copper-assisted chemical etching with inverted pyramidal structures intermediate between texturing and nanopore-type black silicon. *J. Mater. Chem. A*, **2,** 12043–12052 (2014).
28. Hesketh, P. J., Ju, C., Gowda, S., Zanoria, E. & Danyluk, S. Surface Free Energy Model of Silicon Anisotropic Etching. *J. Electrochem. Soc.* **140,** 1080–1085 (1993).
29. Zhang, X. G. *Electrochemistry of Silicon and Its Oxide*. (Kluwer Academic Publishers, New York, 2001).
30. Chyan, O. M. R., Chen, J. J., Chien, H. Y., Sees, J. & Hall, L. Copper Deposition on HF Etched Silicon Surfaces: Morphological and Kinetic Studies. *J. Electrochem. Soc.* **143,** 92–96 (1996).

Acknowledgements

This work was supported by the Ministry of Science and Technology of China (Grant Nos. 2011CB302002 and 2009CB929404), the National Science Foundation of China (Grant Nos. 11174348, 51272280, 11274366, 61204067, and 61306011), the Chinese Academy of Sciences, and the Research Council of Norway in the framework of the IDEAS grant program administrated via the ENERGIX program, as well as OXYDERA equipment grant from the Centre for Materials Science and Nanotechnology at the University of Oslo. The authors would like to thank Profs. X.C.Ma and Q.K.Xue from Tsinghua University for valuable discussion.

Author Contributions

X.L.D., Y.P.L., Z.X.M. and A.K. designed the experiments. Y.W., L.X.Y., Y.P.L., J.Q.L., W.C. and H.L.L. performed the experiments and analyses. Y.W., L.X.Y. and Y.P.L. wrote the paper with A.K. and X.L.D. All authors discussed the results and commented on the manuscript.

Additional Information

Competing financial interests: The authors declare no competing financial interests.

How to cite this article: Wang, Y. *et al.* Maskless inverted pyramid texturization of silicon. *Sci. Rep.* **5**, 10843; doi: 10.1038/srep10843 (2015).

This work is licensed under a Creative Commons Attribution 4.0 International License. The images or other third party material in this article are included in the article's Creative Commons license, unless indicated otherwise in the credit line; if the material is not included under the Creative Commons license, users will need to obtain permission from the license holder to reproduce the material. To view a copy of this license, visit http://creativecommons.org/licenses/by/4.0/